Burgers Turbulence with Large-scale Forcing

Toshiyuki Gotoh[1,*] and Robert H. Kraichnan[2,†]
[1] Department of Systems Engineering, Nagoya Institute of Technology, Showa-ku, Nagoya 466, Japan
[2] 369 Montezuma 108, Santa Fe, NM 87501-2626

(25 March 1998)

Burgers turbulence supported by white-in-time random forcing at low wavenumbers is studied analytically and by computer simulation. The peak of the probability distribution function (pdf) $Q(\xi)$ of velocity gradient ξ is at $\xi = O(\xi_f)$, where ξ_f is a forcing parameter. It is concluded that $Q(\xi)$ displays four asymptotic regimes at Reynolds number $R \gg 1$: (A) $Q(\xi) \sim \xi_f^{-2}\xi \exp(-\xi^3/3\xi_f^3)$ for $\xi \gg \xi_f$ (reduction of large positive ξ by stretching); (B) $Q(\xi) \sim \xi_f^2|\xi|^{-3}$ for $\xi_f \ll -\xi \ll R^{1/2}\xi_f$ (transient inviscid steepening of negative ξ); (C) $Q(\xi) \sim |R\xi|^{-1}$ for $R^{1/2}\xi_f \ll -\xi \ll R\xi_f$ (shoulders of mature shocks); (D) very rapid decay of Q for $-\xi \geq O(R\xi_f)$ (interior of mature shocks). The typical shock width is $O(1/Rk_f)$. If $R^{-1/2} \gg rk_f \gg R^{-1}$, the pdf of velocity difference across an interval r is found be $P(\Delta u, r) \propto r^{-1}Q(\Delta u/r)$ throughout regimes A and B and into the middle of C.

I. INTRODUCTION

A number of papers in the past several years have treated the physics of turbulent solutions of Burgers equation [1–13]. A variety of results on statistics of solutions, sometimes contradictory, have been reported. Burgers turbulence driven by forcing that varies infinitely rapidly in time (white-in-time) was first systematically studied by Chekhlov and Yakhot [2,6]. The present paper is concerned with Burgers turbulence supported by white-in-time forcing that has a compact wavenumber spectrum.

Two processes act upon the velocity field injected by a forcing term: the self-advection of the velocity field steepens negative velocity gradients and reduces positive gradients. The viscous term relaxes the curvature of the velocity field. The effects of each term are easy to treat in isolation, but the combination of the two terms poses nontrivial difficulties.

At large Reynolds numbers, the self advection tends to produce sawtooth structures with smooth ramps of gentle positive velocity gradient and narrow shocks of strong negative gradient. The shock width is $O(\nu/\Delta u)$, where Δu is the jump in velocity across the shock and ν is viscosity. Shocks can interact. A strong shock can move across the domain and swallow weaker structures in its path.

The present paper offers physically motivated approximations on terms in the exact equations of motion for the probability distributions of velocity gradient and velocity difference and examines their consistency. We assume that the forcing has compact spectral support at low wavenumbers and is white in time. The results are tested against computer simulations and the relation to other theoretical approaches is discussed. Four asymptotic regions are predicted at large Reynolds number: a region of large positive gradient where the gradient probability density decreases very rapidly; a region of intermediate negative gradient where the density follows a -3 law; a region of larger intermediate gradient where the density follows a -1 law; and finally an outer region of negative gradient where decay is very rapid. The power-law regions are mediated by transient advective steepening of gradients and the shoulders of mature shocks, respectively, while the outer region represents gradients within strong shocks.

II. STATISTICAL EQUATIONS FOR THE VELOCITY GRADIENT

Burgers equation with forcing is

$$u_t + uu_x = \nu u_{xx} + f, \tag{1}$$

where $u(x,t)$ is a one-dimensional velocity field and $f(x,t)$ is a forcing term. The left side of (1) is the Lagrangian time derivative of u, measured along a fluid-element trajectory. We shall assume that the forcing is white in time, statistically homogeneous and stationary, with compact spectral support concentrated about a wavenumber k_f. Let

$$B = \int_0^t \langle f_x(x,t) f_x(x,s)\rangle \, ds, \tag{2}$$

where $u(x, t = 0) = 0$ and $\langle\ \rangle$ denotes ensemble average. A characteristic forcing strain rate and Reynolds number induced by the forcing may be defined by $\xi_f = B^{1/3}$ and $R = \xi_f/(\nu k_f^2)$. The steady-state values of rms velocity $u_{rms} = \langle u^2\rangle^{1/2}$ and typical shock jump induced by the forcing are both $O(\xi_f/k_f)$. The typical shock width is ν/u_{rms} and the typical velocity gradient $\xi = u_x$ within a shock is $R\xi_f$.

Differentiation of (1) yields

$$\xi_t + u\xi_x = -\xi^2 + \nu\xi_{xx} + f_x. \tag{3}$$

The ξ^2 term in (3) represents advective gradient intensification or diminution along Lagrangian trajectories. An exact equation of motion for the probability distribution function (pdf) $Q(\xi)$ of ξ follows from (3):

$$\frac{\partial Q}{\partial t} - \frac{\partial}{\partial \xi}\left(\xi^2 Q\right) = -\nu\frac{\partial[H(\xi)Q(\xi)]}{\partial \xi} + \xi Q + B\frac{\partial^2 Q}{\partial \xi^2}. \tag{4}$$

Here $H(\xi) \equiv \langle \xi_{xx}|\xi\rangle$ denotes the ensemble mean of ξ_{xx} conditional on fixed ξ. This relation was derived in [1] for zero forcing by following probabilities along Lagrangian trajectories. The B term in (4) expresses in standard fashion the outward diffusion of probability due to white-in-time forcing.

The ξ^2 term in (3) plays two opposed roles. If $\xi < 0$, it intensifies the gradient but, at the same time, squeezes the fluid and thereby decreases the measure along x associated with an interval $d\xi$. If $\xi > 0$, the gradient is decreased but measure is increased by stretching of the fluid. The intensification or diminution of gradient is expressed in (4) by the $\partial(\xi^2 Q)/\partial\xi$ term and the rate of change of measure is expressed by the ξQ term. An identity for homogeneous fields,

$$\frac{\partial}{\partial \xi}\left(\langle u\xi_x|\xi\rangle Q\right) \equiv \xi Q, \tag{5}$$

gives an alternative expression for the rate of change of measure.

III. APPROXIMATIONS FOR ASYMPTOTIC RANGES

The limit $R \to \infty$ suggests the existence of several asymptotic ranges of $Q(\xi)$, whose form can be found if physically-based approximations to the terms of (4) are valid. We shall outline these approximations compactly in this Section, and later address some questions and paradoxes that arise.

First, consider places in the flow, at a given time, where forcing has produced an extraordinarily large positive value $\xi \gg \xi_f$. Stretching should very quickly flatten such regions, suggesting that the ν terms in (3) and (4) can be neglected in comparison to the other terms in a statistically steady state. The Q equation then reduces to

$$B\frac{\partial^2 Q}{\partial \xi^2} + \xi^2\frac{\partial Q}{\partial \xi} + 3\xi Q = 0, \tag{6}$$

The general solution involves $\exp(-\xi^3/3B)$. The solution that vanishes at $\xi = +\infty$ is

$$Q(\xi) \approx C_+\,\xi_f^{-2}\xi\exp(-\xi^3/3B) \quad (\xi \gg \xi_f), \tag{7}$$

where C_+ is a dimensionless constant and the inequality defines the range in which we hope the neglect of viscous effects is justified. The exponential factor in (7) was first found by Polyakov [4], but with a different prefactor.

Next, consider places where $\xi < 0$ and $\xi_f \ll -\xi \ll R\xi_f$. The first inequality implies that the gradient is steepening with a time constant $\ll 1/\xi_f$ and the second inequality makes $|\xi|$ small compared to typical gradients found within a shock. We therefore neglect the ν and B terms in (4), yielding in steady-state

$$\xi^2\frac{\partial Q}{\partial \xi} + 3\xi Q = 0. \tag{8}$$

The solution of physical interest is

$$Q(\xi) \approx C_{-3}\,\xi_f^2|\xi|^{-3} \quad (\xi_f \ll -\xi \ll R^{1/2}\xi_f), \tag{9}$$

where C_{-3} is another dimensionless constant. Again, the inequalities express the range in which we hope our approximations are valid. The second inequality stated in (9) is stronger than called for by the argument just given. This is because the transient steepening contribution (9) to Q is overshadowed in the range $R^{1/2}\xi_f \ll -\xi \ll R\xi_f$ by contributions from the shoulders of the strong, quasi-equilibrium shocks that decay with time constants $O(1/\xi_f)$.

There is a simple physical explanation for (9). Consider a place where forcing has produced negative ξ with $-\xi = O(\xi_f)$ over a region of size $O(1/k_f)$ where ξ_{xx} is small enough that viscous effects are negligible. Steepening of the gradient will carry the gradient to larger negative values and the time in which it is $O(|\xi|)$ will be $O(1/|\xi|)$. Simultaneously, the measure will shrink to $O(\xi_f/|\xi|)$. Thus this process will contribute $O(1/|\xi|^2)$ to $|\xi|Q(\xi)$, the probability of finding the gradient at $O(|\xi|)$. This implies $Q(\xi) \propto |\xi|^{-3}$.

An equilibrium single-shock solution of (1), (3) is $u(x) = -u_s\tanh(u_s x/2\nu)$,

$$\xi(x) = -\left(\frac{u_s^2}{2\nu}\right)\operatorname{sech}^2\left(\frac{u_s x}{2\nu}\right). \tag{10}$$

The jump across the shock is $2u_s$. The measure on x of places with gradient between ξ and $\xi + d\xi$ is $d\xi/|\xi_x|$. By differentiation of (10), the contribution of this shock to $Q(\xi)$ is then

$$Q(\xi) \propto \frac{\nu}{|\xi|\sqrt{u_s^2 - 2\nu|\xi|}} \quad (|\xi| < u_s^2/2\nu). \tag{11}$$

If $u_s = O(u_{rms})$ and $|\xi| \ll R\xi_f$, this is simply $Q(\xi) \propto \nu/u_s|\xi|$.

Now consider a train of such shocks, spaced $1/k_f$ apart, with a uniform gradient $2u_s k_f$ added so that there is no secular change of u. It follows that the normalized total contribution to $Q(\xi)$ for $\xi_f \ll |\xi| \ll R\xi_f$ is $O(1/R|\xi|)$.

The significance of R here is that it measures the ratio of shock spacing to shock width. For $|\xi| \ll R^{1/2}\xi_f$, this contribution to Q is overpowered by (9), but for $|\xi| \gg R^{1/2}\xi_f$, it overpowers (9). Thus the third asymptotic range is

$$Q(\xi) \approx \frac{C_{-1}}{R|\xi|} \quad (R^{1/2}\xi_f \ll -\xi \ll R\xi_f), \tag{12}$$

where C_{-1} is yet another dimensionless constant. This result is unchanged in form if the shocks of fixed jump $2u_s$ are replaced by shocks with a distribution of jump values $u_s = O(u_{rms})$.

The form (12) may also be obtained by approximate dynamic analysis that follows the evolution of those regions of negative gradient that evolve into the shoulders of an equilibrium shock. An example is the mapping closure for Burgers shocks [1].

Equation (11) may be integrated over a distribution $P_s(u_s)$ of shock jumps to get the form of $Q(\xi)$ for $-\xi \geq O(R\xi_f)$, where contributions from within the shocks must dominate Q. Thus,

$$Q(\xi) \approx \frac{C_s u_{rms}}{R|\xi|} \int_{\sqrt{2\nu|\xi|}}^{\infty} \frac{P_s(u_s)du_s}{\sqrt{u_s^2 - 2\nu|\xi|}} \quad (-\xi \geq O(R\xi_f)), \tag{13}$$

where C_s is a dimensionless constant. $P_s(u_s) \propto u_s \exp(-\frac{1}{2}au_s^2/u_{rms}^2)$, where a is a dimensionless constant, is one of the forms for which the integration in (13) is analytic. It yields

$$Q(\xi) \approx \frac{C_s}{R|\xi|} \exp(-a|\xi|R/\xi_f) \quad (-\xi \geq O(R\xi_f)). \tag{14}$$

It happens that the form (14) is also obtained by applying mapping closure to (1) and (3), both in the case of free decay [1] and in the present forced case.

Note that (14) gives an exponential fall-off while the assumed $P_s(u_s)$ falls off as a Gaussian. This is because the gradient in the center of a shock is $-u_s^2/2\nu$. The shock width ν/u_s decreases as u_s increases.

Several authors have concluded that the tail of the pdf of shock jump falls off more rapidly than that of the Gaussian forcing; in particular, $\ln P_s(u_s) \propto -(u_s/u_{rms})^3$ at large u_s [3,8,9]. The reason is that the decay rate of a shock is $O(u_s k_f)$, which increases with increase of u_s. The corresponding prediction for the gradient pdf is $\ln Q(\xi) \propto -(|\xi|R/\xi_f)^{3/2}$ at large negative ξ, instead of (14).

IV. THE CONDITIONAL MEAN OF DISSIPATION

The conditional mean $H(\xi)$ embodies all the difficulty in solving (4). We wish now to examine whether this mean behaves in a way that realizes the asymptotic $R \to \infty$ ranges of $Q(\xi)$ proposed in Sec. III.

The steady-state asymptotic behavior of $H(\xi)$ at $-\xi \gg R\xi_f$ can be inferred immediately if the B term can be neglected in that range. H must balance the remaining two terms, which represent steepening and loss of measure:

$$\nu H(\xi) \approx \xi^2 + \frac{1}{Q(\xi)} \int_{-\infty}^{\xi} Q(\xi')\xi' d\xi'. \tag{15}$$

Note that statistical homogeneity requires $\int_{-\infty}^{\infty} Q(\xi)\xi d\xi = 0$. If $Q(\xi)$ falls off faster than algebraically as $\xi \to -\infty$, then the ξ^2 term in (15) is dominant. The integration in (15) is analytic for the example (14), giving

$$\nu H(\xi) \approx \xi^2 + R\xi_f\xi/a. \tag{16}$$

Paradoxically, $\nu H(\xi)$ plays an important role in (4) at $|\xi| = O(\xi_f)$, however small ν may be. This is because of the contribution from the shoulders of mature shocks. If this is so, how can the H term be negligible for larger negative ξ, as assumed in obtaining (9)?

Differentiation of (10) gives

$$\nu\xi_{xx} = 3\xi^2 + (u_s^2/\nu)\xi. \tag{17}$$

If $u_s = O(u_{rms})$, the second term in (17) is $O(R\xi_f\xi)$, and it dominates the first term for $|\xi| \ll R\xi_f$. Consider the measure, per unit length of x, of the portion of a shock shoulder where $|\xi| = O(\xi_f)$. If the shock spacing is $O(1/k_f)$, this measure is $M_S(|\xi| = O(\xi_f)) = O(R^{-1})$ while the total measure per unit length $M_T(|\xi| = O(\xi_f))$, where $|\xi| = O(\xi_f)$, is $O(1)$. The total measure is dominated by field, freshly injected by the forcing, that has not interacted with shocks. If R is large, $\nu H(\xi = O(\xi_f))Q(\xi = O(\xi_f))$ is dominated by the contribution $(u_s^2/\nu)\xi = O(R\xi_f^2)$ from the shock shoulders. The corresponding contribution to $\nu H(\xi)$ is $O(R\xi_f^2)M_S/M_T$. Since $M_S/M_T = O(R^{-1})$, this implies that the shock shoulders make an $O(R^{-1}R\xi_f^2)$ contribution to $H(\xi)$ for ξ negative and $O(\xi_f)$. Thus the ν term in (4) is the same order as the $\partial(\xi^2 Q)/\partial\xi$ term for such ξ. It is independent of R as $R \to \infty$.

Next consider the putative range (9). Here the dominant part of ξ_{xx} within the shock shoulders is again $\propto \xi$, while by (12) the contribution of the shoulders to $Q(\xi)$ is $\propto 1/\xi$. The contribution of the shoulders to $H(\xi)Q(\xi)$ is again the dominant one. This contribution thus goes like $\xi\xi^{-1}$ and is independent of ξ to leading order. The ν term in (4) vanishes to leading order when the ξ differentiation is performed. This is consistent with the neglect of the ν term in deriving (9).

The regions outside the shoulders have negligible $\nu\xi_{xx}$ at large R. A relative-measure estimate, like that above, then implies $H(\xi) \propto \xi^3$ for $\xi_f \ll -\xi \ll R^{1/2}\xi_f$. $H(\xi)$ grows with $|\xi|$ throughout the range (9), but neglect of $\partial[H(\xi)Q(\xi)]/\partial\xi$ appears to be valid.

V. STATISTICAL EQUATIONS FOR VELOCITY DIFFERENCES

Let $P(\Delta u, r)$ be the pdf of $u(x+r,t) - u(x,t)$, where r is always taken positive. If $z = \Delta u/r$, then $P(\Delta u, r) = \tilde{Q}(z,r)/r$ where $\tilde{Q}$ is the pdf of z. An equation of motion for P is obtained by following Lagrangian trajectories as in the derivation [1] of (4). Two trajectories must be followed simultaneously in the present case. The result is

$$\frac{\partial P}{\partial t} = -\nu \frac{\partial}{\partial \Delta u}\left[\left\langle \left(\frac{\partial^2}{\partial x^2} + \frac{\partial^2}{\partial x'^2}\right)\Delta u \middle| \Delta u \right\rangle P\right] - \Delta u \frac{\partial P}{\partial r}$$

$$+ \left\langle \left(\frac{\partial \Delta u}{\partial x'} - \frac{\partial \Delta u}{\partial x}\right) \middle| \Delta u \right\rangle P + F(r)\frac{\partial^2 P}{\partial \Delta u^2}, \qquad (18)$$

where $F(r) = \int_0^t [f(x+r,t)-f(x,t)][f(x+r,s)-f(x,s)]ds$ and $x' = x + r$. The next-to-last term in (18) expresses the change of measure at the points x and x'. It contains $\partial u(x,t)/\partial x$ and $\partial u(x',t)/\partial x'$. Instead of the $\xi^2 Q$ gradient intensification term in (4), there is now the $\partial P/\partial r$ term. It expresses the change of the label r carried by the velocity difference between the two fluid elements as they move closer ($\Delta u < 0$) or apart ($\Delta u > 0$).

An equation for $\tilde{Q}$ equivalent to (18) may be written as

$$\frac{\partial \tilde{Q}}{\partial t} = r^{-2}F(r)\frac{\partial^2 \tilde{Q}}{\partial z^2} + z^2\frac{\partial \tilde{Q}}{\partial z} + z\tilde{Q} - zr\frac{\partial \tilde{Q}}{\partial r}$$

$$+ M(z,r)\tilde{Q} - \nu\frac{\partial[\tilde{H}(z,r)\tilde{Q}]}{\partial z}, \qquad (19)$$

where $z = \Delta u/r$,

$$M(z) = 2z + 2r\,\langle \partial z/\partial r | z\rangle\,,$$

$$\tilde{H}(z) = \langle u_{xx}(x',t) - u_{xx}(x,t)|z\rangle\,/r. \qquad (20)$$

In (20), M has been re-expressed by use of the identity $\partial\bar{u}/\partial\bar{x} \equiv \partial\Delta u/\partial r$, where $\bar{u} = \frac{1}{2}[u(x,t)+u(x',t)]$. M can be further tranformed [14] by use of the homogeneous-field identity [15]

$$\langle \partial z/\partial r|z\rangle \equiv -\frac{1}{\tilde{Q}(z,r)}\int_{-\infty}^{z}\frac{\partial \tilde{Q}(z',r)}{r}dz'. \qquad (21)$$

This expresses the advective contributions to (19) entirely in terms of $\tilde{Q}$, at the expense of creating an integro-differential equation. An equation equivalent to (19) was obtained by Polyakov [4] by exploiting translation invariance of the equation of motion for the characteristic function (Fourier transform) of $\tilde{Q}$.

If the limit $r \to 0$ is taken, $z \to \xi$ and $\tilde{Q}(z,r) \to Q(\xi)$, which is independent of r. Also, $\tilde{H}(z,r) \to H(\xi)$ and $r^{-2}F(r) \to B$. Then (19) goes into (4).

If r is greater than typical shock widths and z is large enough, the right side of (21) is dominated by contributions from shocks such that one of the two points x and x' lies in the shock front while the other lies outside. The integration limits in (21) express the fact that all shocks with jumps $\geq \Delta u$ contribute.

The pdf of $z = \Delta u/r$ should approximate that of ξ if, in the line-segments of length r that contribute significantly at a given z, ξ fluctuates negligibly over the distance r. For $\xi > 0$ or $|\xi| \sim \xi_f$, a plausible sufficient condition for this is $rk_f \ll 1$. For $-\xi \gg \xi_f$, the typical spatial scale of variation of ξ has been decreased by squeezing to $\sim \xi_f/k_f|\xi|$. The requirement for negligible variation of ξ over r is then $r \ll \xi_f/k_f|\xi|$, which can be rewritten as $rk_f \ll \xi_f/|\xi|$ or $r|\xi| \ll u_{rms}$. This excludes Δu values due to the presence of a typical shock within r. The condition for the pdfs of z and ξ to fall on each other throughout the -3 range is consequently $rk_f \ll R^{-1/2}$. If $R^{-1/2} \gg rk_f \gg R^{-1}$, the collapse of the pdfs of z and ξ should extend into the -1 range. In general, if $rk_f \ll 1$ the pdf of z should fall below that of ξ at negative ξ large enough that $rk_f \ll \xi_f/|\xi|$ is violated.

VI. COMPARISON WITH SIMULATIONS

Computer solution of (1) by an SX4 machine was carried out on a cyclic domain of $N = 2^{17}$ to $N = 2^{20}$ points with unit spacing. The forcing had a wavenumber spectrum of form (A) $k^2\exp[-(k/k_f)^2]$ or (B) $k^4\exp[-(k/k_f)^2]$. The forcing field at each time step was an independent realization of Gaussian statistics. The initial spectrum for u had the form $k^2\exp[-(k/k_f)^2]$, with variance chosen to minimize transients in u_{rms}. The simulations were continued until the statistics of interest were stationary ($\sim 10^5$ time steps). The steady state Reynolds numbers $R = u_{rms}/\nu k_f$ ranged from 15 to 18000. The integrations were performed using second-order schemes in x and t. Table I shows the simulation parameters for the runs reported here. $\langle R\rangle$ is the approximate time average of R over the period in which $Q(\xi)$ exhibited a statistically stationary state. Statistics were averaged over sets of similar runs that differed only in the random numbers used in realizing the forcing and initial velocity spectra. For Runs 3–5, additional averaging was performed over time in the statistically stationary state.

Fig. 1 shows $\log_{10}[\langle\xi^2\rangle^{1/2}Q(\xi)]$ plotted against $\xi/\langle\xi^2\rangle^{1/2}$ for $R \sim 15, 1200, 18000$ (Runs 3–5). Note the increase in sharpness of the peak as R increases. Fig. 2 shows the central region of $\xi_f Q(\xi)$ plotted against ξ/ξ_f for three runs with forcing spectrum (B), $R \sim 15, 1200, 18000$ (Runs 3–5) and Run 1, with forcing spectrum (A) at $R \sim 15$. With the ξ_f scaling, the central

region is substantially insensitive to change of forcing spectrum or R.

Fig. 3 shows superimposed plots, for $R \sim 1200$ (Run 4) and $R \sim 18000$ (Run 5), of $\log_{10}[\xi_f Q(\xi)]$ against $\log(|\xi|/\xi_f)$ for $\xi < 0$. The straight lines have slopes of -3 and -1. The $R \sim 18000$ data seem consistent with the existence of the proposed asymptotic ranges (9) and (12) but clearly even higher R values would be needed to make an unambiguous case.

The steady-state pdf equation, obtained by setting $\partial Q/\partial t = 0$ in (4) has interesting stability properties. If the dissipation term $\nu\partial[H(\xi)Q(\xi)]/\partial\xi$ is omitted, the general solution is analytically accessible. It contains exponential factors that make numerical solution violently unstable if carried out in the negative ξ direction and highly stable if carried out in the positive ξ direction. A consequence is that the central peak of Q is quite insensitive to the form assigned to the ν term.

Fig. 4 shows the central part of $\xi_f Q(\xi)$ plotted against ξ/ξ_f for four cases: (a) the $R \sim 1200$ simulation (Run 4); (b) the left-to-right numerical solution of (4) in steady state with dissipation term set to zero; (c) the left-to-right numerical solution with dissipation term taken as $0.45\xi_f Q(\xi)$; (d) the left-to-right solution with dissipation term taken as $0.8609\xi_f Q(\xi)/(1 + \xi^2/\xi_f^2)$. The three numerical solutions were started at large negative ξ, where $Q(\xi) \propto \xi^{-3}$ and normalized to unit probability.

The first notable thing about Fig. 4 is that case (b) is so close to case (a). It is has a small, unphysical negative region at $\xi > 0$, but nevertheless lies near (a) over the peak region. The forms (c) and (d) for the dissipation are even closer to (a). They decay according to (7) as $\xi \to \infty$.

Case (c) is the case $a = 0$ of the closure approximation $\nu\partial[HQ]/\partial\xi = (a\xi + b\xi_f)Q$ introduced by Polyakov [4] and studied also by Boldyrev [12]. This closure was obtained as a low-order truncation of the operator-product expansion associated with Burgers equation.

For our present purposes, (c) and (d) are simply two functional forms that serve to increase $\partial^2 Q/\partial\xi^2$ for $|\xi| \sim \xi_f$. The choice of a functional form for this purpose is only weakly constrained, but the numerical coefficient is not. It is fixed by the requirements that $Q(\xi)$ be positive for all ξ and decay faster than algebraically as $\xi \to \infty$ [4,12]. The second requirement is satisfied also by case (b). If the numerical coefficients in cases (c) and (d) are increased, the right tail of $Q(\xi)$ decays like ξ^{-3} instead of like (7). If the coefficients are decreased, a negative region like that in case (b) is produced. The numbers 0.45 and 0.8609 stated above are approximations to the exact marginal values.

It was noted in Sec. V that viscous effects from the shoulders of mature shocks are present at $|\xi| \sim \xi_f$ even as $R \to \infty$. Fig. 4 suggests that the principal consequence of these effects in the Q equation are not upon the form of the central peak, whose shape is remarkably stable, but upon the decaying region of Q at larger positive ξ.

The putative asymptotic range (7) is difficult to define well by simulation. $Q(\xi)$ decays so rapidly with increase of ξ that very large sample sets are needed. Fig. 5 is a plot of $3B\partial(\ln Q)/\partial(\xi^3)$ vs ξ^3/B for Run 2, a $R \sim 15$ simulation with forcing spectrum (B). The $\exp(-\xi^3/3B)$ factor in (7) seems supported. But the approach to the horizontal asymptote is protracted, consistent with the presence of a positive-power prefactor.

A definitive test of the prefactor exponent in (7) is more difficult. Fig. 6 is a plot of $3\partial(\ln Q)/\partial(\ln \xi^3)$ against ξ^3/B. If the $\exp(-\xi^3/3B)$ factor is present in Q, the prefactor exponent is given by the intercept at $\xi^3 = 0$ of a straight line drawn through this plot at large ξ^3.

In order to help resolve the prefactor, we have included in Figs. 5 and 6 curves corresponding to a mapping approximation [1] carried out with the same ν and forcing parameters as the simulation. A detailed description of the approximation for the forced case will be given elsewhere. We report now is that it yields (7) at infinite R but gives $Q(\xi) \propto \xi_f^{-2}\xi\exp(-\mathrm{const}\,\nu\xi/u_{rms}^2 - \xi^3/3B)$ for $\xi \gg \xi_f$ at finite R. The simulation and mapping curves in Fig. 6 lie close to each other. Straight lines drawn through the outer parts of both curves ($10 \le \xi^3/B \le 15$) intercept the vertical axis near 1.

It is also difficult in the simulations to resolve the conditional mean $H(\xi)$ cleanly for large negative ξ. In addition to the need for large sample sets, the x grid must be sufficiently fine to resolve unusually narrow shocks. Fig. 7 shows $\nu H(\xi)/\xi_f^2$ plotted against ξ/ξ_f ($\xi < 0$) for Run 3, which has high resolution. Also shown are the parabolas $\nu H(\xi) = \xi^2$ and $\nu H(\xi) = \xi^2 + \xi_C\xi$, where ξ_C is the value at which the simulation data for $H(\xi)$ change sign. The latter function is an approximation suggested by (17). The second term in the asymptotic relation (15) obviously is negative for $\xi < 0$. This implies that ξ^2 is an upper bound to $\nu H(\xi)$ for large negative ξ.

Fig. 8 shows data for $\xi_f r P(\Delta u, r)$ from the $R \sim 1200$ simulation (Run 4) plotted against $\Delta u/r\xi_f$ for a number of values of r. Also shown is $\xi_f Q(\xi)$ plotted against ξ/ξ_f. As r decreases, the curves for P follow that for Q over an increasingly long range of $\Delta u/r$. At the smaller r values, this collapse extends into the -1 range of the Q curve. The envelope of the knees of the P curves, beyond the region of collapse, follows a line of slope -2 on the log-log plot. This is because the regions of large $\Delta u/r$ are dominated by contributions from the mature shocks, and scale with u_{rms}. The latter scaling is clearly shown in Fig. 9, where $P(\Delta u, r)/\xi_f r$ is plotted against $\Delta u/u_{rms}$. The outer regions of the curves collapse.

Figs. 10 and 11 are similar to Figs. 8 and 9 except that they show data for $R \sim 18000$ (Run 5).

VII. DISCUSSION

The theory of Burgers equation with low-wavenumber, white-in-time forcing has had a variety of treatments, and there has been a variety of predictions. The $\exp(-\xi^3/3B)$ factor in the right tail of $Q(\xi)$ seems generally accepted. It was first predicted by Polyakov [4] on the basis of the truncation $\nu\partial[HQ]/\partial\xi = (a\xi + b\xi_f)Q$ of the operator product expansion, as noted in Sec. VI. Later it was recovered by instanton analysis [8–10].

Equation (4) is exact. If the ν term in (4) can be neglected in the right tail, it follows that the prefactor is ξ, as shown in (7). Neglect of viscous effects in the right tail is plausible but not obviously justified. One must consider the effects of possible proximity of regions of large positive ξ to the shoulders of strong shocks.

All values $a \neq 0$ in Polyakov's closure give significant viscous effects in the right tail, with the consequence that the predicted prefactor is ξ^{1-a}. Instanton analysis that neglects viscous effects at the start [10] must yield the ξ prefactor. However, extraction of the prefactor from instanton analysis is a delicate matter that requires careful treatment of fluctuations about the saddle point.

There is also disagreement about the exponent of the putative power-law range for intermediate negative ξ. The predictions have ranged from -2 [6,7] to $-7/2$ [11]. Polyakov's closure gives $q = 3 - a$; values $0 \leq a \leq 1$ have been considered [4,12].

As discussed in Sec. IV, the dissipation contribution from the shoulders of a distribution of ideal Burgers shocks gives $H(\xi) \propto |\xi|^3$ if $Q(\xi) \propto |\xi|^{-3}$, so that the ν term in (4) vanishes to leading order, as required for consistency. If $Q(\xi) \propto |\xi|^{-q}$ $(q \neq 3)$, (4) in steady state requires

$$\nu H(\xi) \approx \frac{3-q}{2-q}\xi^2. \tag{22}$$

Thus $H(\xi)$ is negative if $2 < q < 3$ and positive if $q > 3$ or $q < 2$. If R is large, contributions to H for the range $|\xi| \ll R\xi_f$ in question can come only from the shoulders of shocks. The profile of ξ in a shock is a negative peak so that, whatever the precise profile, the curvature of the shoulders is negative and the contribution to $H(\xi)$ therefore is negative. This appears to rule out $q > 3$ and $q < 2$. Values $q \neq 3$ imply shock profiles different from that of the ideal Burgers shock (10).

Values $q \leq 2$ are ruled out for another reason. Homogeneity requires $\int_{-\infty}^{\infty} Q(\xi)\xi\, d\xi = 0$. The contribution to this integral from $\xi > 0$ is finite and independent of R as $R \to \infty$, if the right tail of Q falls off rapidly in the fashion generally accepted. But if the negative-ξ power-law range extends from $|\xi| = O(\xi_f)$ to $|\xi| = O(R^c\xi_f)$ where $c > 0$, then the contribution of this range to the integral is negative and becomes infinite as $R \to \infty$. Since the contribution from the left tail beyond the powerlaw range is also negative, the homogeneity condition cannot be satisfied in the limit.

The value $q = 7/2$ was proposed in the course of an analysis of the inviscid Burgers equation [11]. One thing established rigorously in this work is that the mean spacing of strong shocks is $O(1/k_f)$ if the forcing has compact spectral support about k_f. The value $q = 7/2$ was obtained by examining the behavior of $u(x,t)$ in the immediate vicinity of the formation of an incipient shock, and then looking back in time at the structure of the regions that were destined to form these vicinities. We believe that this procedure yields a biased sample of the preshock velocity field. Equation (9) is intended to describe the probability balance associated with the evolution of all regions of negative ξ. Only a zero-measure set of these regions is destined to form part of the immediate vicinity of an incipient shock in the limit $R \to \infty$.

One effect not taken into account in the derivation of (9) is passage of a mature shock through a region where ξ is steepening. Such passage can wipe out the local process. Since negative ξ increases in magnitude until it either forms part of a shock or is wiped out by a shock collision, the collision process should make $Q(\xi)$ fall off more rapidly than (9) with increase of $|\xi|$. The rate of increase of ξ within a fluid element, before viscous effects are felt and neglecting forcing effects, is $\xi(t) \propto \xi_0/(1 - |\xi_0|t)$, where t is measured from some effective initial time when $\xi = \xi_0$. The times at which $|\xi|$ is large compared to $|\xi_0|$ are all crowded into an interval $\ll 1/|\xi_0|$ at $t = O(1/|\xi_0|)$. The mean time between shock collisions is $O(1/k_f u_{rms})$. Because of the crowding in time, the the collision probability changes very slowly with $|\xi|$ for $|\xi| \gg \xi_f$, and we do not expect the collision effects to change the power law in (9).

We are indebted to S. A. Boldyrev, S. Chen, A. Chekhlov, M. Chertkov, G. Falkovich, V. Lebedev, A. M. Polyakov, B. Shraiman, Y. Sinai, and V. Yakhot for valuable discussions and correspondence. T.G.'s work was supported in part by Grant-in-Aid for Scientific Research C,09640260 from the Ministry of Education, Science, Sports and Culture of Japan, and by the Computational Science and Engineering, Research for the Future Program, Japan Society for the Promotion of Science. R.H.K.'s work was supported by the United States Department of Energy, Office of Basic Energy Sciences, under Grant DE-FG03-90ER14118.

TABLE I. SIMULATION PARAMETERS

Run	$\langle R\rangle$	$u_{rms}(t=0)$	Spectrum	k_f	ν	N	dt	B	Set size
1	15	1	A	0.02	10/3	2^{17}	0.1	4×10^{-6}	102
2	15	1	B	0.02	10/3	2^{17}	0.1	7.2×10^{-6}	102
3	15	1	B	0.02	10/3	2^{20}	0.1	7.2×10^{-6}	102
4	1200	1	B	5×10^{-4}	2	2^{18}	0.1	2×10^{-10}	102
5	18000	1	B	5×10^{-5}	2.2	2^{20}	0.2	5×10^{-13}	61

* Electronic address: gotoh@system.nitech.ac.jp
† Electronic address: rhk@lanl.gov

[1] T. Gotoh and R. H. Kraichnan, "Statistics of decaying Burgers Turbulence," Phys. Fluids A **5**, 445 (1993); T. Gotoh, "Inertial range statistics of Burgers turbulence," Phys. Fluids **6**, 3985 (1994).
[2] A. Chekhlov and V. Yakhot, "Kolmogorov turbulence in a random-force-driven Burgers equation," Phys. Rev. E, **51**, 2739 (1995); A. Chekhlov and V. Yakhot, "Kolmogorov turbulence in a random-force-driven Burgers equation: anomalous scaling and probability density functions," Phys. Rev. E **52**, 5681 (1995).
[3] M. Avellaneda, R. Ryan, and Weinan E, "PDFs for velocity and velocity gradients in Burgers turbulence," Phys. Fluids **7**, 3067 (1995).
[4] A. M. Polyakov, "Turbulence without pressure," Phys. Rev. E **52**, 6183 (1995).
[5] J.-P. Bouchaud, M. Mézard, and G. Parisi, "Scaling and intermittency in Burgers turbulence," Phys. Rev. E **52**, 3656 (1995).
[6] V. Yakhot and A. Chekhlov, "Algebraic tails of probability functions in the random-force-driven Burgers turbulence," Phys. Rev. Lett. **77**, 3118 (1996).
[7] J.-P. Bouchaud and M. Mézard, "Velocity fluctuations in forced Burgers turbulence," Phys. Rev. E **54**, 5116 (1996).
[8] G. Falkovich, I. Kolokolov, V. Lebedev, and A. Migdal, "Instantons and intermittency," Phys. Rev. E **54**, 4896 (1996).
[9] E. Balkovsky, G. Falkovich, I. Kolokolov, and V. Lebedev, "Intermittency of Burgers turbulence," Phys. Rev. Lett. **78**, 1452 (1997).
[10] V. Gurarie and A. Migdal, "Instantons in the Burgers equation," Phys. Rev. E **54**, 4908 (1996).
[11] Weinan E, K. Khanin, A, Mazel, and Y. Sinai, "Probability distribution functions for the random forced Burgers equation," Phys. Rev. Lett. **78**, 1904 (1997).
[12] S. A. Boldyrev, "Velocity-difference probability density functions for Burgers turbulence," Phys. Rev. E **55**, 6907 (1997).
[13] S. N. Gurbatov, S. I. Simdyankin, E. Aurell, U. Frisch, and G. Toth, "On the decay of Burgers turbulence," J. Fluid Mech. **344**, 339 (1997).
[14] S. A. Boldyrev, private communication (1997).
[15] Y. Kimura and R. H. Kraichnan, "Statistics of an advected passive scalar," Phys. Fluids A **5**, 2264 (1993), Sec. II.

FIGURE CAPTIONS

FIG. 1. Plot of $\log_{10}[\langle\xi^2\rangle^{1/2} Q(\xi)]$ against $\xi/\langle\xi^2\rangle^{1/2}$ for three sets of runs with forcing spectrum (B) and $R \sim 15$ (Run3, light dashes), 1200 (Run 4, heavy dashes) and 18000 (Run 5, solid line).

FIG. 2. The central region of $\xi_f Q(\xi)$ plotted against ξ/ξ_f for the three runs with forcing spectrum (B), $R \sim 15$ (Run 3, light solid line), 1200 (Run 4, heavy solid line), 18000 (Run 5, heavy dashes), and a run with forcing spectrum (A) at $R \sim 15$ (Run 1, light dashes).

FIG. 3. Plot of $\log_{10}[\xi_f Q(\xi)]$ against $\log(|\xi|/\xi_f)$ for $\xi < 0$. $R \sim 15$ (Run 3, light dashes) $R \sim 1200$ (Run 4, heavy dashes) and $R \sim 18000$ (Run 5, solid line) are shown. The straight lines have slopes of -3 and -1.

FIG. 4. The central part of $\xi_f Q(\xi)$ plotted against ξ/ξ_f for four cases: (a) the $R \sim 1200$ simulation (Run 4, heavy solid line); (b) the left-to-right numerical solution of (4) in steady state with dissipation term set to zero (light solid line); (c) the left-to-right numerical solution with dissipation term taken as $0.45\xi_f Q(\xi)$ (heavy dashes); (d) the left-to-right solution with dissipation term taken as $0.8609\xi_f Q(\xi)/(1+\xi^2/xi_f^2)$ (light dashes).

FIG. 5. Plot of $3B\partial(\ln Q)/\partial(\xi^3)$ vs ξ^3/B for a $R \sim 15$ simulation (Run 2, solid line). Dashed line is a mapping approximation.

FIG. 6. Plot of $3\partial(\ln Q)/\partial(\ln \xi^3)$ against ξ^3/B (Run 2, solid line). Dashed line is a mapping approximation.

FIG. 7. Plot of $\nu H(\xi)/\xi_f^2$ against negative values of ξ/ξ_f for a $R \sim 15$ simulation (Run 3, solid line). Also shown are the parabolas $(\xi/\xi_f)^2$ (light dashes) and $(\xi^2 + \xi_C \xi)/\xi_f^2$ (heavy dashes).

FIG. 8. Plot of $\xi_f r P(\Delta u, r)$ from the $R \sim 1200$ simulation (Run 4) against $\Delta u/r\xi_f$ (dashed lines) for values of r that increase by factors of $\sqrt{2}$ from $rk_f \approx .008$ to $rk_f \approx 0.72$. The curve that is highest on the left side is $rk_f \approx 0.72$. Also shown is $\xi_f Q(\xi)$ plotted against ξ/ξ_f (solid line).

FIG. 9. $P(\Delta u, r)/\xi_f r$ plotted against ud/u_{rms} for the $R \sim 1200$ run. The curves denote the r values of Fig. 8.

FIG. 10. Plot of $\xi_f r P(\Delta u, r)$ from the $R \sim 18000$ simulation (Run 5) against $\Delta u/r\xi_f$ (dashed lines) for values of r that increase from $rk_f \approx 0.0016$ to $rk_f \approx 0.82$. The curve that is highest on the left side is $rk_f \approx 0.82$. Also shown is $\xi_f Q(\xi)$ plotted against ξ/ξ_f (solid line).

FIG. 11. $P(\Delta u, r)/\xi_f r$ plotted against $\Delta u/u_{rms}$ for the $R \sim 18000$ run. The curves denote the r values of Fig. 10.

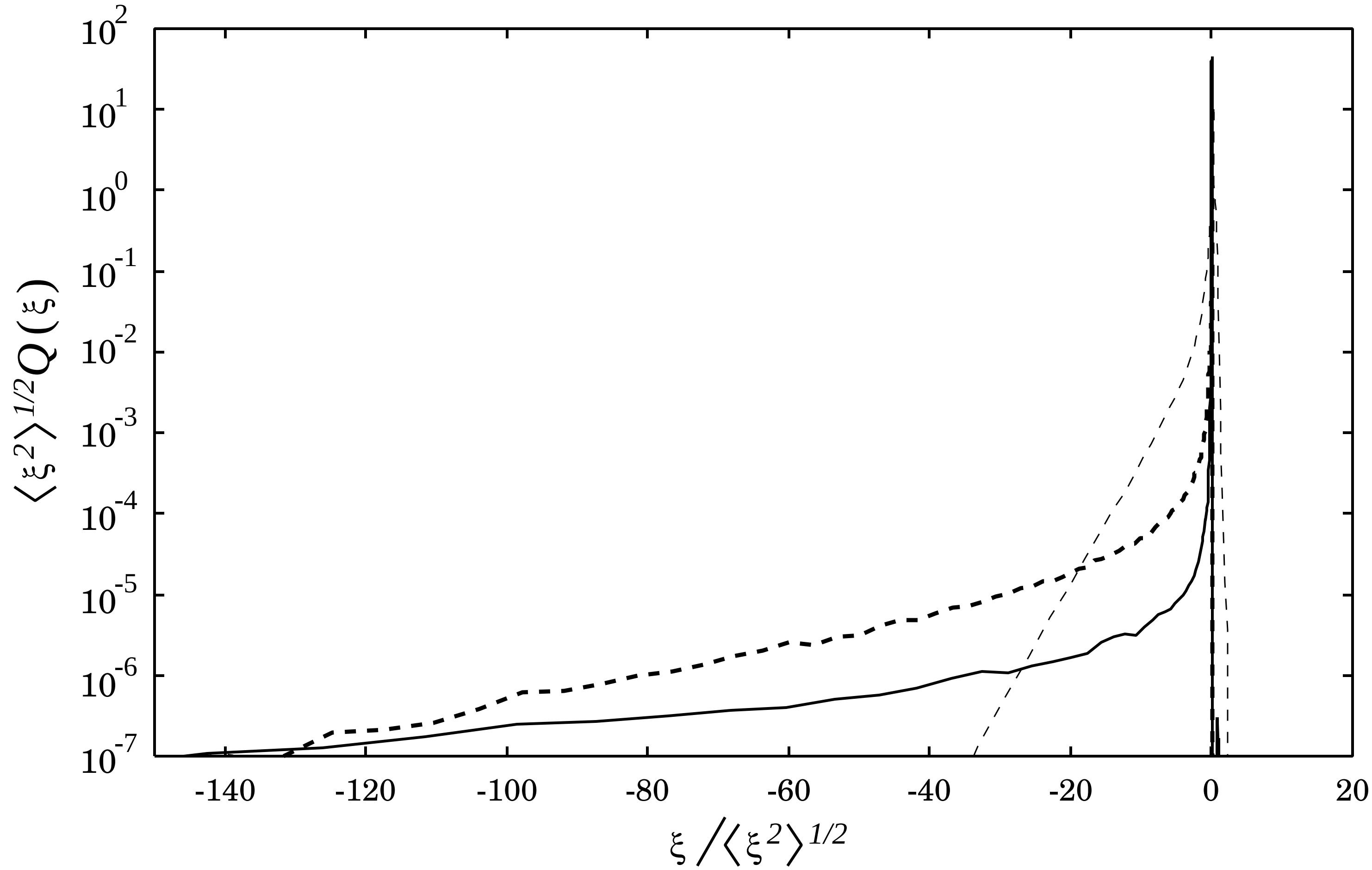

10^{2}
10^{1}
10^{0}
10^{-1}
10^{-2}
10^{-3}
10^{-4}
10^{-5}
10^{-6}
10^{-7}
-140
-120
-100
-80
-60
-40
-20
0
20
$\langle \xi^2 \rangle^{1/2} Q(\xi)$
$\xi / \langle \xi^2 \rangle^{1/2}$

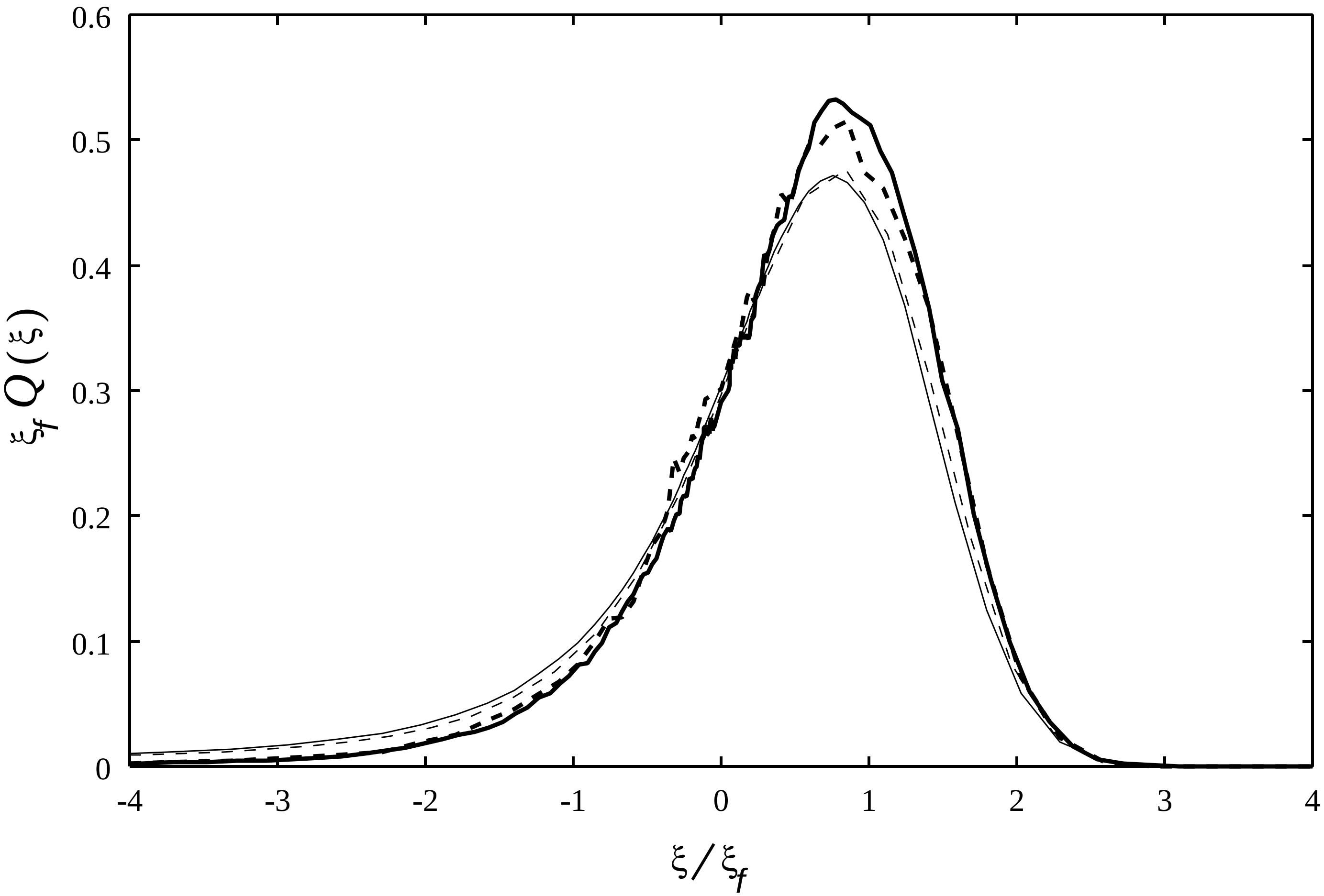

0.6
0.5
0.4
0.3
0.2
0.1
0
-4
-3
-2
-1
0
1
2
3
4
$\xi_f\, Q(\xi)$
ξ/ξ_f

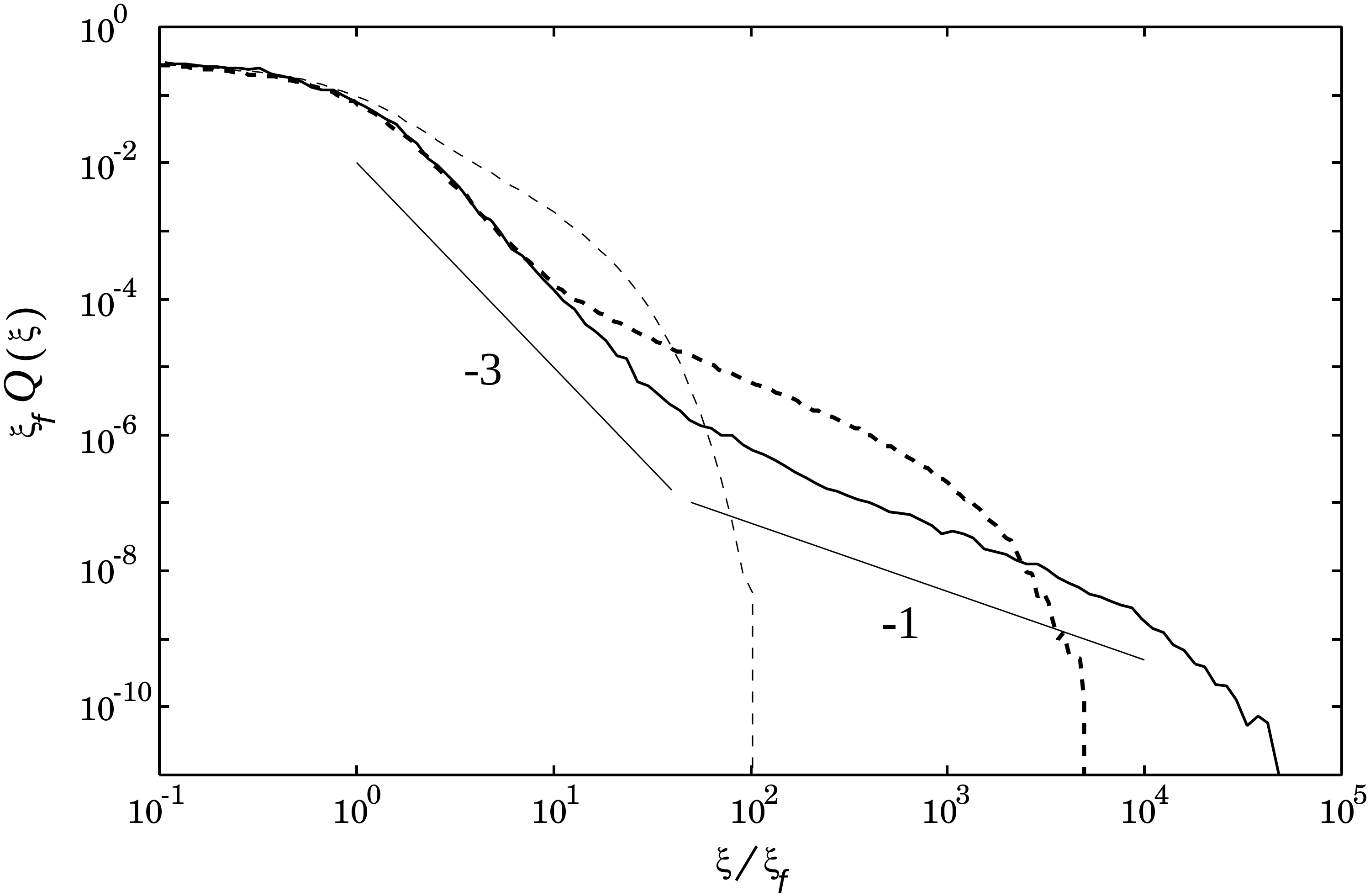

10^{0}
10^{-2}
10^{-4}
10^{-6}
10^{-8}
10^{-10}
$\xi_f Q(\xi)$
-3
-1
10^{-1}
10^{0}
10^{1}
10^{2}
10^{3}
10^{4}
10^{5}
ξ/ξ_f

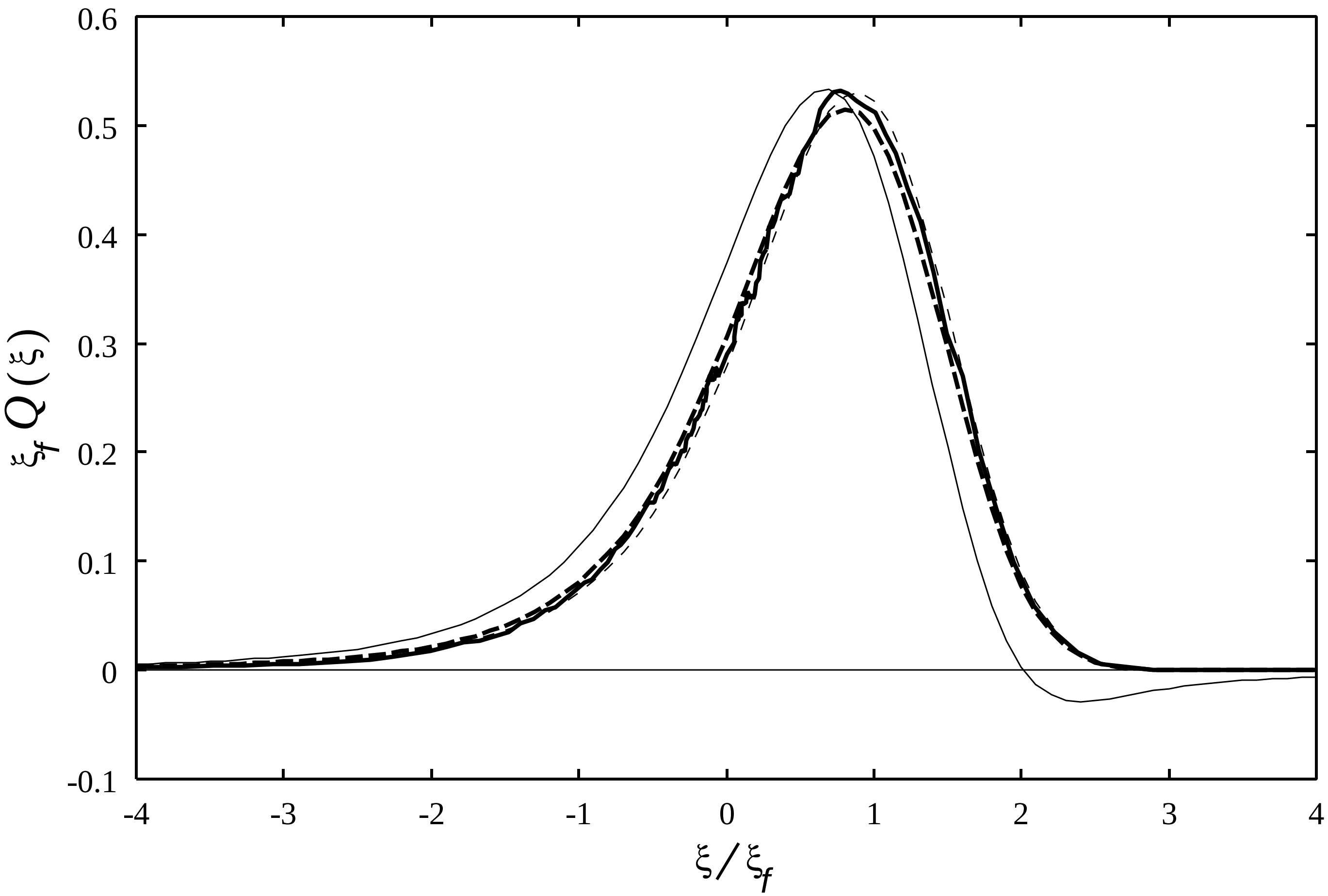
0.6
0.5
0.4
0.3
0.2
0.1
0
-0.1
-4
-3
-2
-1
0
1
2
3
4
$\xi_f\, Q(\xi)$
ξ/ξ_f

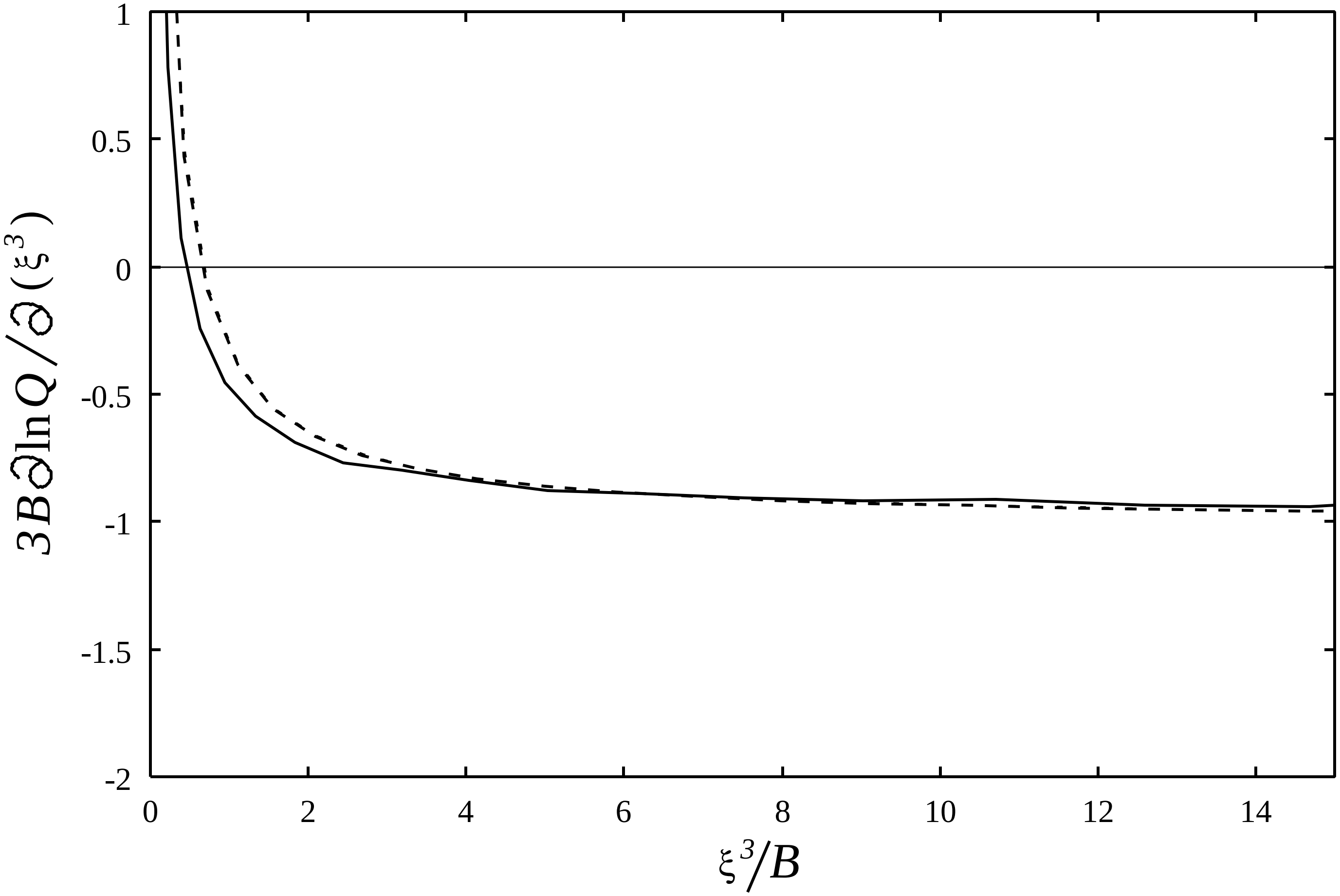

1
0.5
0
-0.5
-1
-1.5
-2
0
2
4
6
8
10
12
14
$3B\partial \ln Q/\partial(\xi^3)$
ξ^3/B

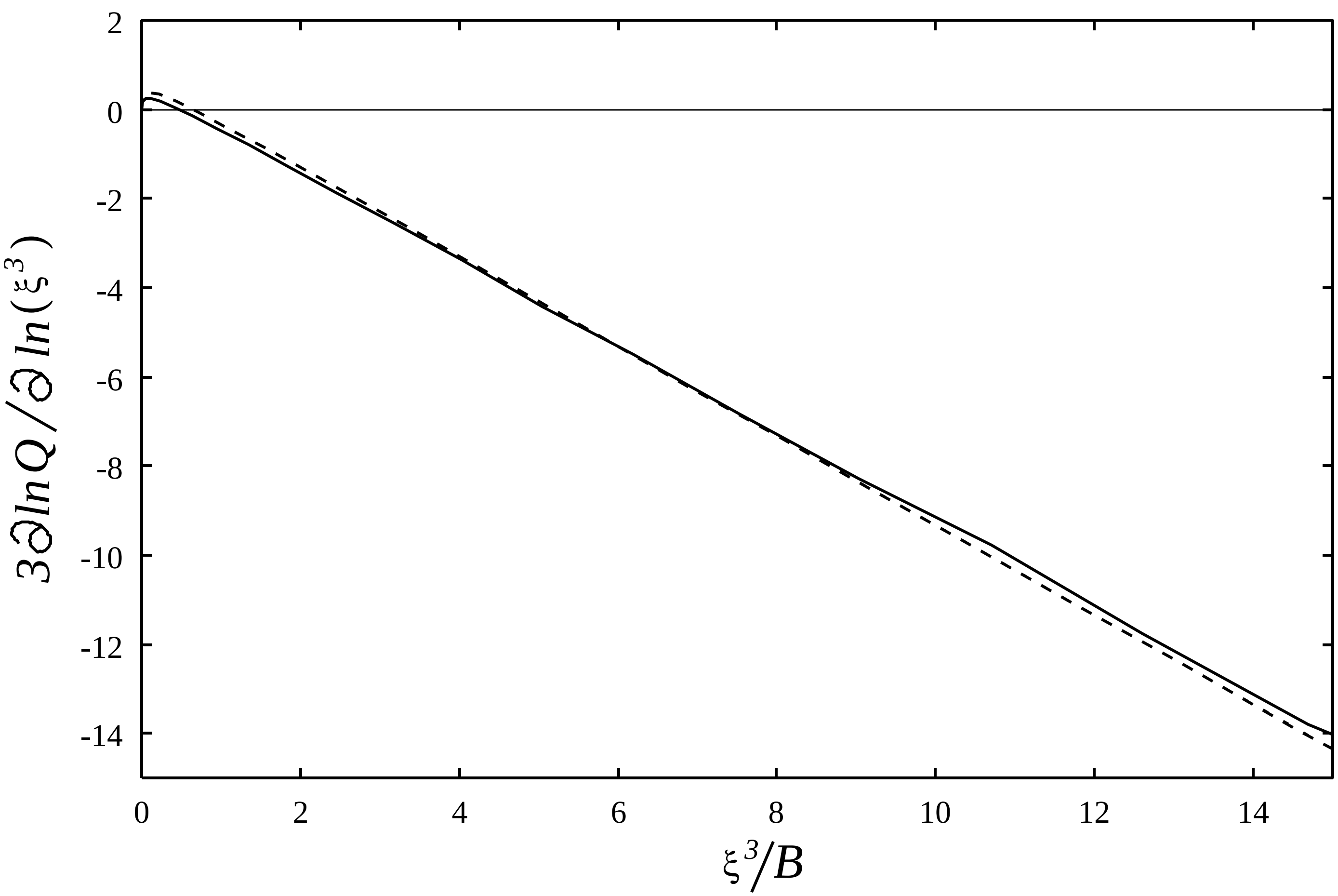

2
0
-2
-4
-6
-8
-10
-12
-14
0
2
4
6
8
10
12
14
$3\partial lnQ/\partial ln(\xi^3)$
ξ^3/B

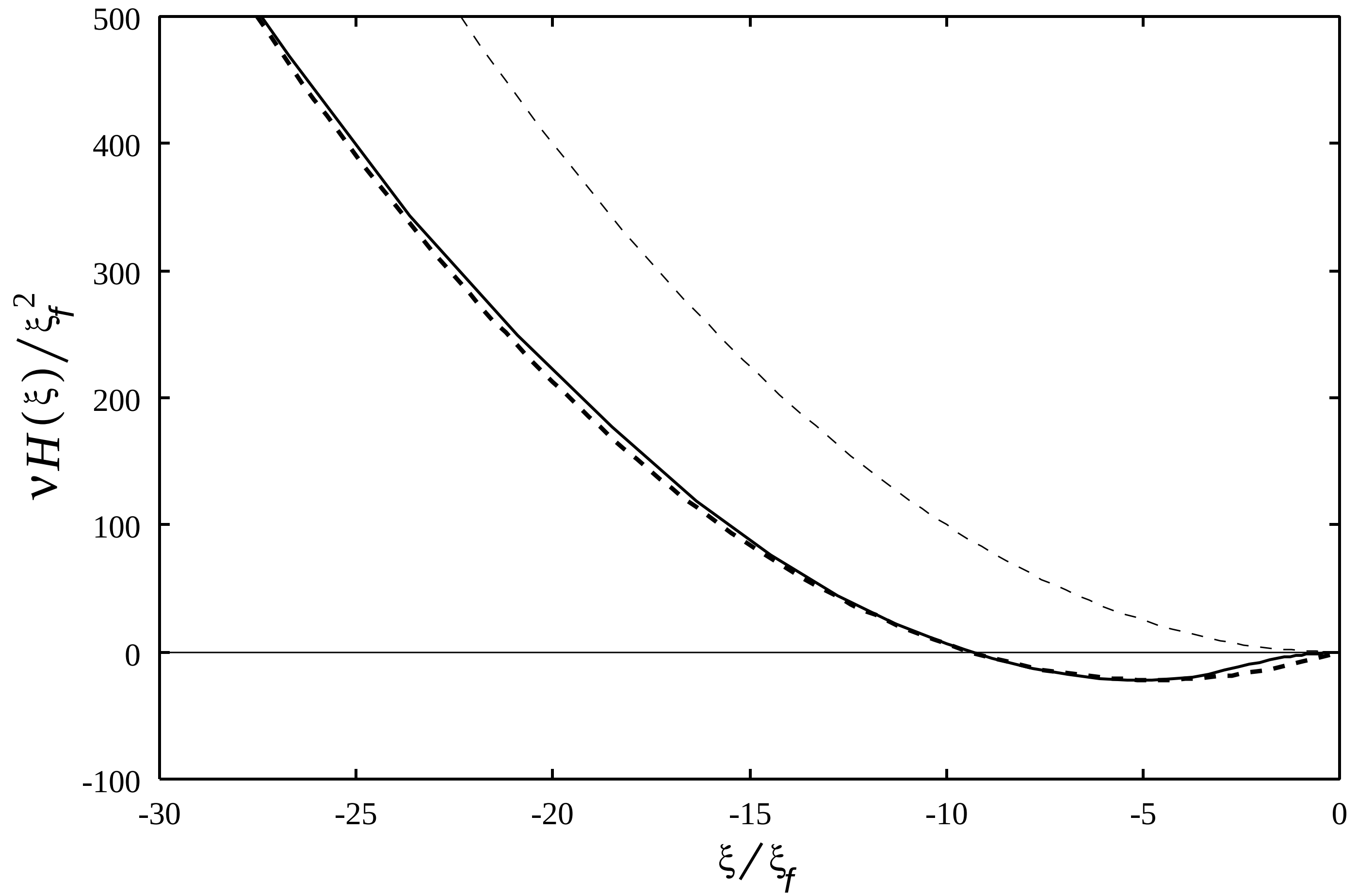
500
400
300
200
100
0
-100
-30
-25
-20
-15
-10
-5
0
$\nu H(\xi)/\xi_f^2$
ξ/ξ_f

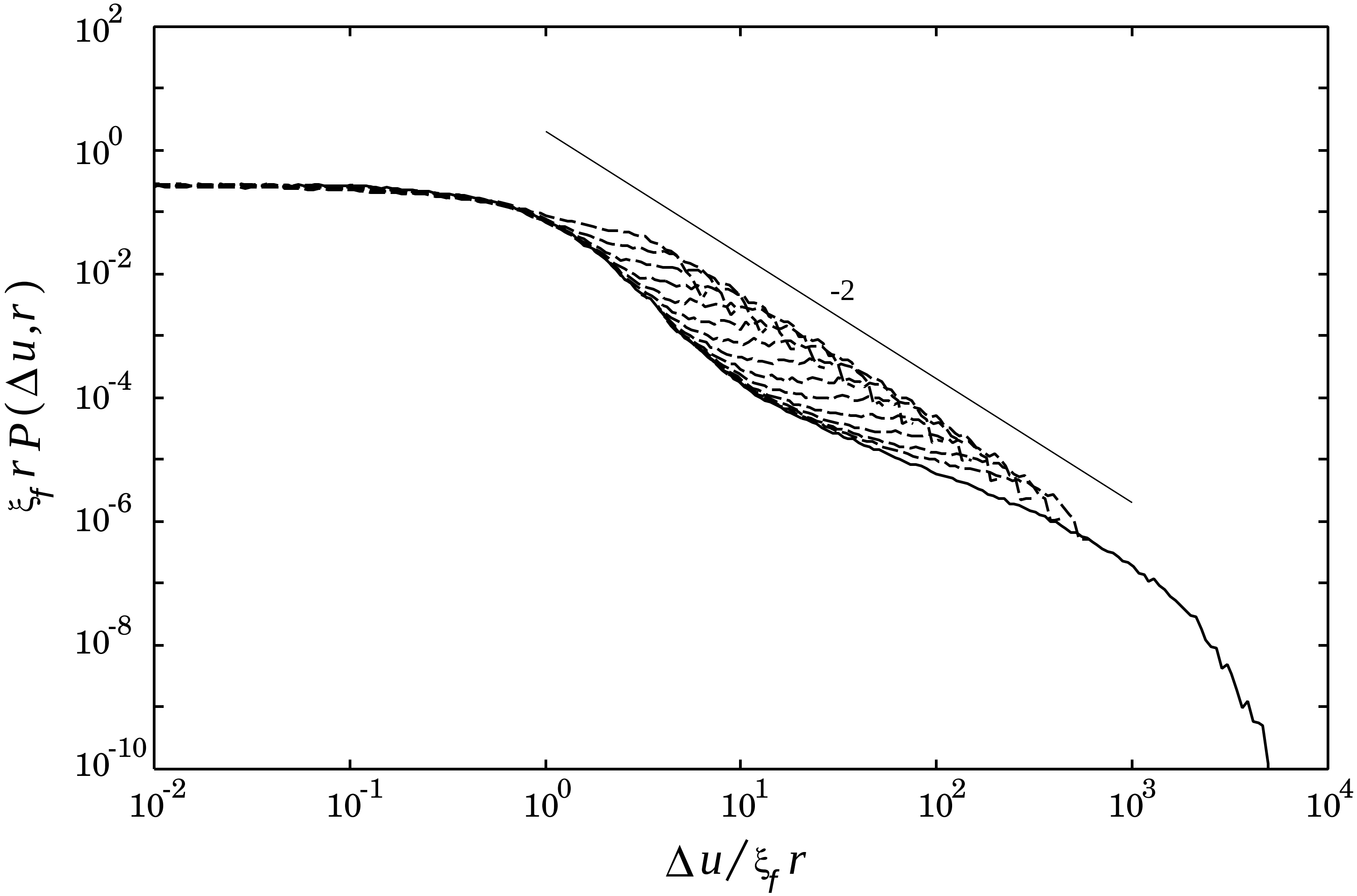

10^{2}
10^{0}
10^{-2}
10^{-4}
10^{-6}
10^{-8}
10^{-10}
10^{-2}
10^{-1}
10^{0}
10^{1}
10^{2}
10^{3}
10^{4}
-2
$\xi_f \, r \, P(\Delta u, r)$
$\Delta u / \xi_f \, r$

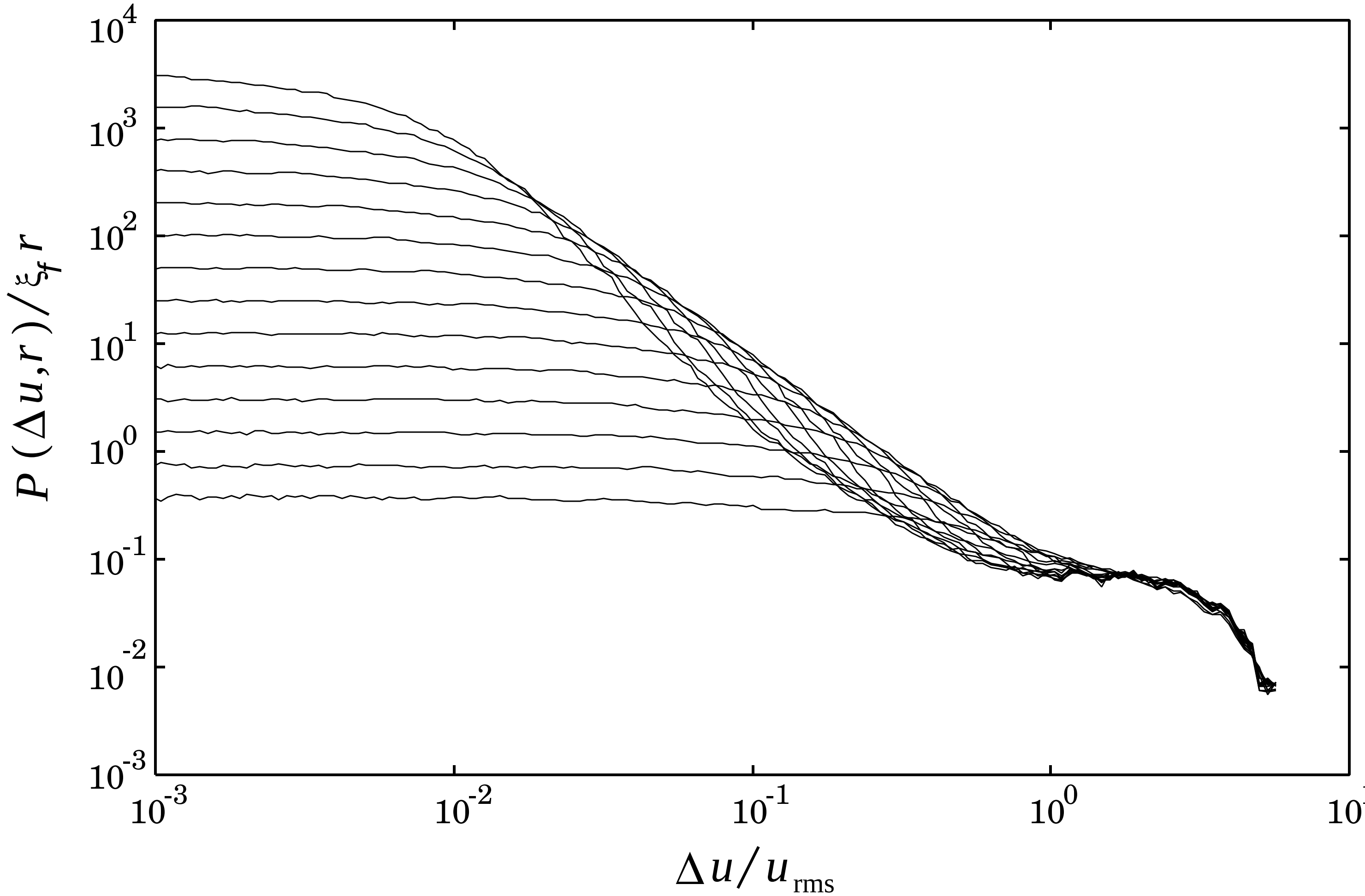

10^{4}
10^{3}
10^{2}
10^{1}
10^{0}
10^{-1}
10^{-2}
10^{-3}
$P\,(\Delta u, r)/\xi_f\, r$
10^{-3}
10^{-2}
10^{-1}
10^{0}
10^{1}
$\Delta u/u_{\mathrm{rms}}$

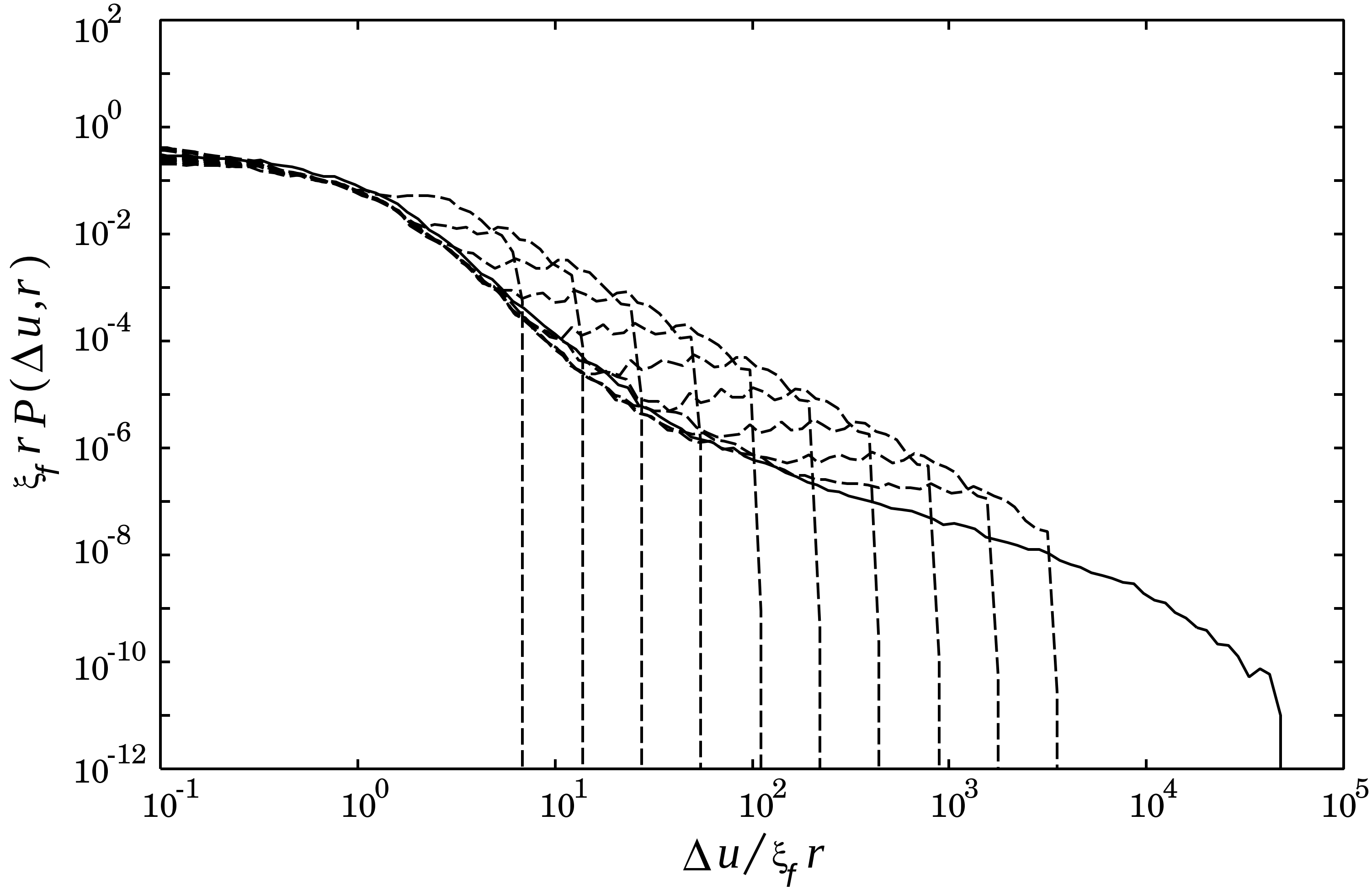

10^{2}
10^{0}
10^{-2}
10^{-4}
10^{-6}
10^{-8}
10^{-10}
10^{-12}
10^{-1}
10^{0}
10^{1}
10^{2}
10^{3}
10^{4}
10^{5}
$\xi_f\, r\, P(\Delta u, r)$
$\Delta u/\xi_f\, r$

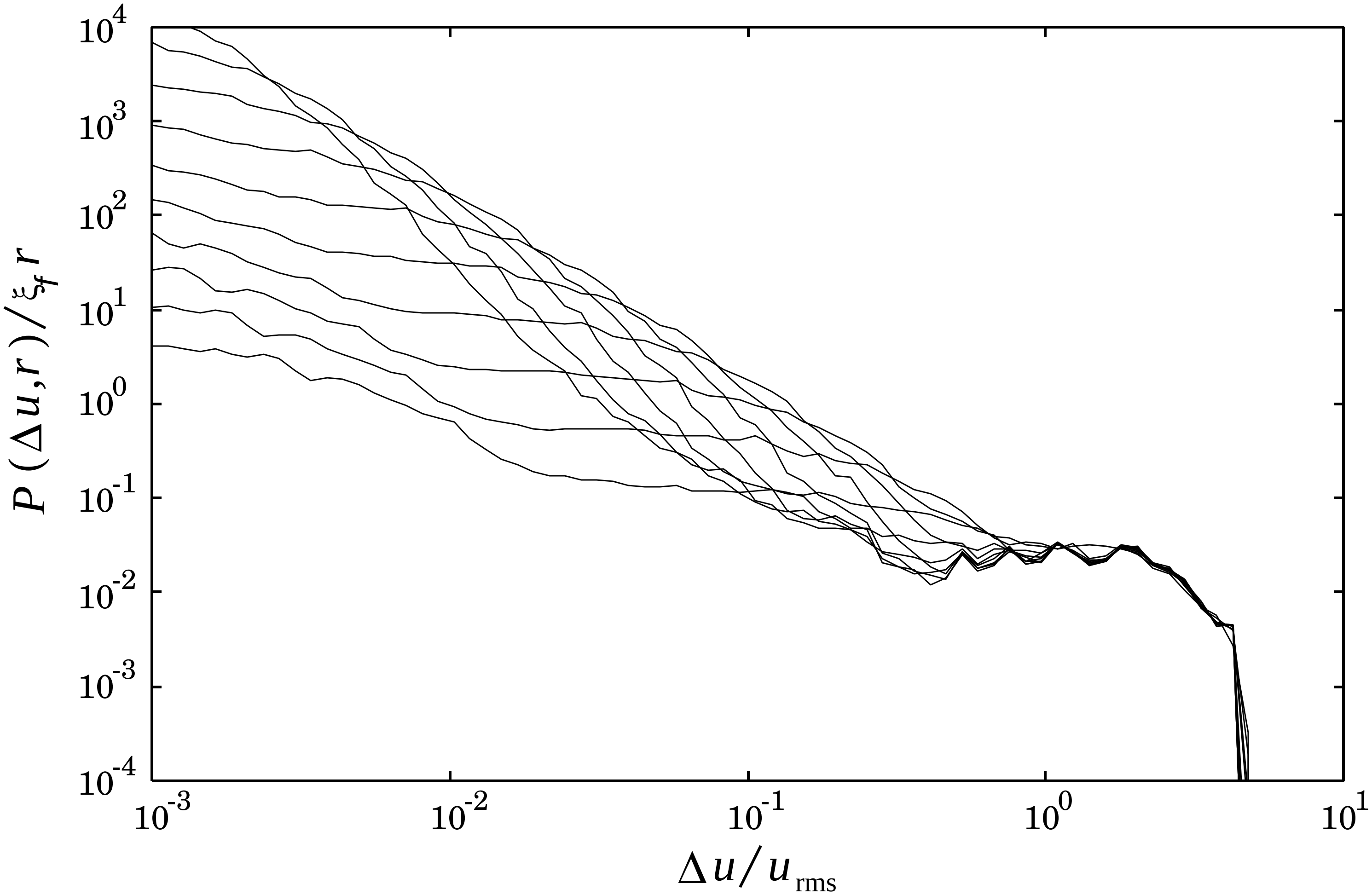

10^4
10^3
10^2
10^1
10^0
10^{-1}
10^{-2}
10^{-3}
10^{-4}
$P\,(\Delta u, r)/\xi_f\, r$
10^{-3}
10^{-2}
10^{-1}
10^0
10^1
$\Delta u/u_{\mathrm{rms}}$